Materials Today Bio 32 (2025) 101789

Contents lists available at ScienceDirect

Materials Today Bio

journal homepage: www.journals.elsevier.com/materials-today-bio

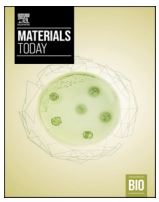

Macrophage membrane functionalized composite microspheres promote bone regeneration in periodontitis via manipulating inflammation reversing-osteogenesis coupling

Rui Song [a,1], Zhuo Wan [b,1], Xiaojing Yuan [a,*], Nan Wang [c], Yike Gao [a], Linxue Zhang [a], Huihui Ren [a], Yu Jin [a], Xiya Liu [a], Jingyi Sang [a], Zuoying Yuan [d,**], Yuming Zhao [a,***]

[a] Department of Pediatrics, Peking University School and Hospital of Stomatology, National Center for Stomatology, National Clinical Research Center for Oral Diseases, National Engineering Research Center of Oral Biomaterials and Digital Medical Devices, Beijing Key Laboratory of Digital Stomatology, Research Center of Engineering and Technology for Computerized Dentistry Ministry of Health, NMPA Key Laboratory for Dental Materials, Beijing, 100081, PR China
[b] Department of Mechanics and Engineering Science, and Beijing Innovation Center for Engineering Science and Advanced Technology, College of Engineering, Peking University, Beijing, 100871, PR China
[c] Department of Stomatology, Peking University Third Hospital, Beijing, 100191, PR China
[d] Center of Basic Medical Research, Institute of Medical Innovation and Research, Peking University Third Hospital, Beijing, 100191, PR China

ARTICLE INFO

Keywords:
Periodontitis
Macrophage membranes
Composite microspheres
Osteogenesis
Immunomodulation

ABSTRACT

Periodontitis is characterized by inflammation and alveolar bone loss, primarily caused by immune cells activated by oral bacteria, leading to an imbalance between osteogenesis and bone resorption. Traditional treatments have limited efficacy, which has led to the exploration of regulating the immune microenvironment and utilizing tissue engineering methods as new research directions. Our study demonstrates that macrophage membranes, activated by LPS and IFN-γ, can effectively neutralize inflammatory factors. By coating the poly-L-lysine (PLL) modified poly (lactic-co-glycolic acid) (PLGA)/β-TCP microspheres with such macrophage membrane vesicles, the MM@PPT microspheres regulate intercellular responses by inhibiting macrophage M1 polarization and osteoclast differentiation, promoting M2 polarization, and enhancing osteogenic differentiation of bone marrow stromal cells (BMSCs) even in an inflammatory environment. By injecting the MM@PPT into sites of periodontitis induced bone resorption, it is found that they can effectively promote bone regeneration by modulating the immune-regeneration microenvironment. This work not only highlights the potential of MM@PPT microspheres in promoting alveolar bone regeneration but also provides insights into how these microspheres modulate cell behavior and interactions. The findings of this study offer novel therapeutic strategies for promoting alveolar bone repair in periodontitis.

1. Introduction

Periodontitis is one of the most common oral diseases manifested as periodontal tissue inflammation and alveolar bone destruction, ultimately resulting in tooth mobility and loss [1,2]. The etiology and pathogenesis of periodontitis are multifaceted, among which immune cells activated by oral bacteria are the main cause of producing inflammatory factors that disrupt the balance between osteogenesis and bone resorption [3]. Periodontal tissue inflammation can be managed with local medications and procedures such as scaling and root planning, followed by regenerative surgeries to repair damaged bone tissue. Nevertheless, treatment outcomes are limited [4,5].

Macrophages in periodontal tissues play a pivotal role in maintaining tissue homeostasis as a key component of innate immunity. In addition to macrophages, bone marrow mesenchymal stem cells (BMSCs) are also present in the periodontal bone defect area and can regulate macrophage phenotypes and functions [6,7]. However, after infection by pathogens, macrophages polarize to the M1 phenotype and produce

* Corresponding author.
** Corresponding author.
*** Corresponding author.
E-mail addresses: fatulousfie@126.com (X. Yuan), zy_yuan@pku.edu.cn (Z. Yuan), yuming_zhao@hotmail.com (Y. Zhao).
[1] R. Song and Z. Wan contributed equally to this work.

https://doi.org/10.1016/j.mtbio.2025.101789
Received 20 January 2025; Received in revised form 2 April 2025; Accepted 21 April 2025
Available online 22 April 2025

many inflammatory factors (e.g., tumor necrosis factor-alpha (TNF-α), interleukin-1 (IL-1) and interleukin-6 (IL-6)), inhibiting the activity of osteoblasts and osteogenesis of BMSCs, and promoting the activation of osteoclasts, leading to alveolar bone resorption [8,9]. On the other hand, the conditional medium of BMSCs has been reported to modulate the macrophage phenotype and inhibit the activation of osteoclasts [10]. Therefore, the neutralization of inflammatory factors and modulating of dynamic interactions among macrophages/osteoclasts and BMSCs are crucial for initiating the healing of inflammation bone defects.

Macrophage membranes possess receptors such as the interleukin-6 receptor (IL-6R) and tumor necrosis factor-alpha receptor (TNF-αR). Macrophage membrane-derived vesicles which are approximately 200 nm in size and retain the surface receptors of the source macrophage membrane, have been utilized to neutralize inflammation and improve the microenvironment through ligand-receptor interactions [11–13]. For example, RAW264.7 cells membrane–functionalized poly (lactic--co-glycolic acid) (PLGA) nanodecoys can neutralize receptor activator of nuclear factor-κ B Ligand (RANKL) and TNF-α, respectively inhibiting osteoclastogenesis and promoting osteoblastogenesis, thereby reversing the progression of osteoporosis in the ovariectomized (OVX) mouse model [14]. After treated by lipopolysaccharide (LPS), macrophage membrane functionalized nanoparticles (LMNP) demonstrate strong sponge-like absorption capacity for interferon-γ (IFN-γ) and IL-6. It inhibits the excessive activation of macrophages by suppressing the JAK/STAT signaling pathway both *in vitro* and *in vivo*, effectively alleviating symptoms related to Hemophagocytic Lymphohistiocytosis (HLH), such as cytopenia, hepatosplenomegaly, and liver and kidney dysfunction [15]. Hence, the role of macrophage membrane vesicles as decoys for inflammatory factors shows their potential application in treating periodontitis-related diseases. After neutralizing the inflammatory factors in the periodontal microenvironment, it is necessary to regulate the polarization state of macrophages further to pro-regenerative M2 phenotype, which can enhance the osteogenesis of MSCs by secreting growth factors such as transforming growth factor beta (TGF-β) and platelet-derived growth factor (PDGF), thereby promoting bone regeneration [16].

Bone resorption in periodontal tissues often presents an irregular shape, making it difficult for traditional bulk biomaterials to adapt to irregular bone defects [17]. Microsphere-type biomaterials, as injectable microscale scaffold materials [18–21], can be easily injected into defect sites and adapt to defects in various shapes, providing a room that facilitates the migration, proliferation, and osteogenesis of MSCs and/or osteoblast [22–24]. β-tricalcium phosphate (β-TCP), which displays a high similarity in structure and solubility to bone mineral, is easy to be replaced by new bone, and has emerged as one of the most attractive bone-graft materials that can be used instead of hydroxyapatite (HAp). During the degradation process of β-TCP, calcium and phosphate ions are rapidly released, which in turn stimulates the gene expression of osteoblasts, thereby facilitating the maturation of new bone tissue [25,26]. In our previous work, we constructed PLGA/β-TCP microspheres with a particle size of approximately 15 μm, which are biodegradable and effectively promote the assembly and osteogenesis of stem cell aggregates, leading to efficient craniofacial bone regeneration [27]. Additionally, β-TCP can reduce inflammation by regulating macrophages to polarize to the M2 phenotype [28]. Poly-lysine (PLL) can be bonded to negatively charged macrophage membranes (MM) through electrostatic interactions. For example, PLL functionalized microribbon (μRB) scaffolds absorb mensenchymal stem cell membrane (MSCM), and the retention rate of MSCM was remained to be ~82 % after 2 weeks incubation *in vitro* [29]. PLL-coated PLGA/β-TCP microspheres functionalized with macrophage membrane vesicles rich in inflammatory factor receptors are expected to be an innovative strategy for restoring the immune microenvironment of periodontal bone defects and promoting bone regeneration.

Here, we first stimulated RAW264.7 cells with LPS and IFN-γ to maximize the number of inflammatory factor receptors on their membrane vesicles. By coating the poly-L-lysine (PLL) modified PLGA/β-TCP microspheres with macrophage membrane vesicles, MM@PPT microspheres were obtained. MM@PPT microspheres act as agents to clear inflammatory factors, modulate the phenotype of macrophages from M1 to M2, and inhibit the osteoclast activation of RANKL-induced macrophages. Furthermore, MM@PPT microspheres promote the osteogenic differentiation of BMSCs and mediate the crosstalk between macrophages and BMSCs, promoting alveolar bone regeneration (Scheme 1). Finally, rat periodontitis was established to identify the feasibility of using MM@PPT microspheres in achieving bone regeneration by modulating the immune-regeneration microenvironment.

2. Materials and methods

2.1. Materials

PLGA (lactic acid: glycolic acid = 75:25, molecular weight = 50,000) was purchased from Shandong Pharmaceutical Science Experimental Factory, and β-TCP (particle size approximately 10 nm) was kindly provided by the Institute of Metal Research, Chinese Academy of Sciences. Other reagents/solvents were purchased from Aladdin (China), unless specifically noted.

2.2. Cell culture

RAW264.7 cells were purchased from (Puno Science, China) and were cultured in high-glucose Dulbecco's modified Eagle medium (DMEM, Gibco, USA) supplemented with 10 % fetal bovine serum (FBS), penicillin (100 U/mL), and streptomycin (100 μg/mL). RAW264.7 cells were pretreated for 24 h with LPS (100 ng/mL) or LPS (100 ng/mL) + IFN-γ (10 ng/mL) before the extraction of macrophage membrane vesicles. BMSCs: Four-week-old SD male rats were euthanized under excessive anesthesia. After soaking in 75 % ethanol, bilateral hind legs were harvested, and after removing muscle tissue, the joint heads of the femurs were cut off. The joint cavity was washed with α-MEM containing 2X antibiotics and 20 % FBS until the bone appeared white. The collected bone marrow fluid was seeded into culture dishes and incubated in a cell incubator. After 48 h, the suspended culture medium was removed, and the medium was changed to continue the culture. When the cell density reached 80 % in the culture dish, the cells were passaged. All BMSCs used in this study were in P3.

2.3. Detection of cytokine receptor expression in macrophages by flow cytometry

To detect the differences in cytokine receptor expression between PBS-treated, LPS-treated, and LPS + IFN-γ-treated macrophages, cells were collected and washed with PBS. The cell suspension was incubated with Phycoerythrin (PE)-conjugated anti-mouse CD126 (IL-6Rα chain) and PE-conjugated anti-mouse CD120α (TNF R Type I/p55) antibodies at 4 °C for 30 min. Afterwards, cells were washed with PBS and analyzed by flow cytometry (Beckman Coulter, USA). Data were analyzed using FlowJo software.

2.4. Western blot analysis of cytokine receptors in macrophages

To investigate the differences in cytokine receptor protein expression among PBS-treated, LPS-treated, and LPS + IFN-γ-treated macrophages, Western blot analysis was performed. Macrophages were collected and lysed with Radio immunoprecipitation assay lysis buffer (RIPA buffer) containing protease inhibitors. Protein concentrations were determined using a BCA assay kit (Thermo, USA) and mixed with loading buffer, followed by heating at 95 °C for 5 min. For each group, 15 μg of protein was loaded into a 10 % SDS-PAGE gel, which was subjected to electrophoresis at 80V for 30 min and then at 120V for 1 h. Subsequently, Enhanced ChemiLuminescence (ECL) substrate was added to the

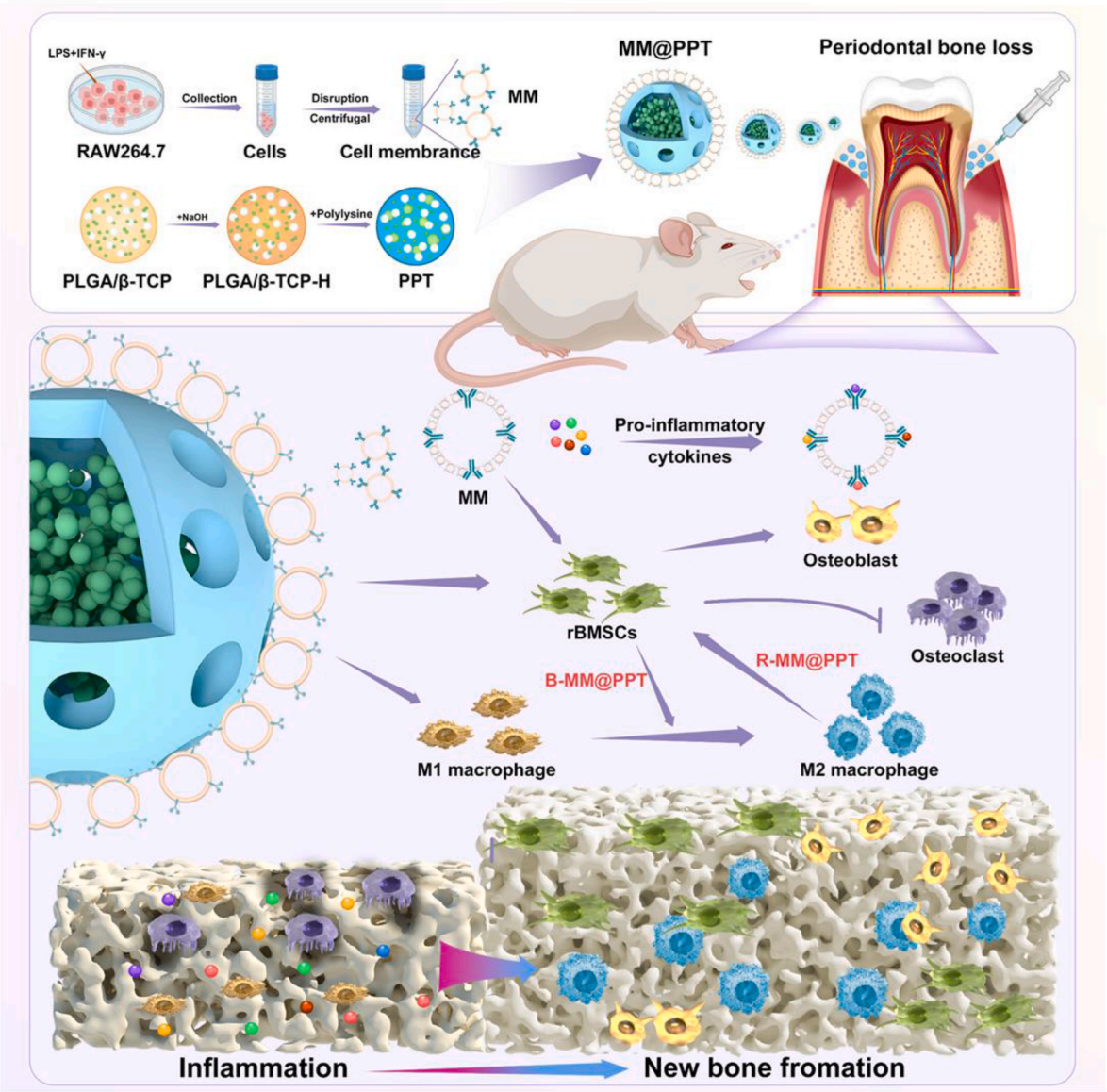

Scheme. 1. Schematic illustration showing the design of MM@PPT for alveolar bone regeneration in periodontitis. MM@PPT consists of macrophage membrane vesicles and PLGA microspheres containing β-TCP, which are surface-modified with poly-L-lysine (PLL). This system effectively modulates the balance between osteogenesis and osteoclastogenesis, creating a beneficial immune microenvironment at the defect site to promote the regeneration of alveolar bone.

membrane surface, and the expression levels of cytokine receptors TNF-αR (CD120a, Proteintech, Wuhan) and IL-6R (CD126, 1:1000, Proteintech, Wuhan) were observed using the imaging system.

2.5. Extraction and characterization of macrophage membrane vesicles

The collection and extraction of cell membranes were performed using previously reported methods [30]. Briefly, the macrophages were collected and gently resuspended in an appropriate volume of ice-cold PBS after pretreatment. The cells were centrifuged at 600 g for 5 min to precipitate the cells, followed by another centrifugation at 1500 rpm for 5 min. Cell membrane proteins were extracted from RAW264.7 cells using a cell membrane protein extraction kit (Beyotime, China). One milliliter of membrane protein extraction reagent A, pre-added with Phenylmethanesulfonylfluoride or phenylmethylsulfonyl fluoride (PMSF), was added to 20 to 50 million cells, and the cells were gently and thoroughly resuspended. The mixture was placed on ice for 10–15 min. A glass homogenizer was used to disrupt the cells. The mixture was centrifuged at 700 g for 10 min at 4 °C, and the supernatant was carefully collected into a new centrifuge tube. The supernatant was centrifuged at 14,000 g for 30 min at 4 °C to pellet the cell membrane fragments.

To obtain macrophage membrane vesicles, the cell membrane was subjected to sealed treatment in a closed glass bottle using a water bath ultrasound device at 100 W for 5 min (Kunshan Ultrasonic Instrument Co., Ltd). The formation of the cell membrane vesicles and their zeta potential analysis were confirmed using transmission electron microscopy (TEM; Hitachi HT7700, Japan), dynamic light scattering (DLS; Delsa Nano, Beckman Coulter, USA), and nanoparticle tracking analysis (NTA; Particle Metrix ZetaVIEW S/N 17–310, Germany). The membrane protein content was measured using BCA assay kit (Beyotime). The collected cell membranes were stored at −80 °C for further use.

2.6. Cytokine neutralization assay

To evaluate the cytokine binding capacity of macrophages stimulated with M0, LPS, and LPS + IFN-γ, different concentrations of macrophage membrane vesicles (10, 50, 100, 500 μg/mL) were mixed

with PBS, TNF-α (85 pg/mL), and IL-6 (360 pg/mL) and incubated at 37 °C for 30 min. The samples were centrifuged at 16,000×*g* for 15 min to remove cell membrane vesicles, and the cytokines in the supernatant were quantitatively analyzed using ELISA (MultiSciences (LiankeBio), Hangzhou).

2.7. Preparation of MM@PPT microspheres

The preparation and characterization of PLGA/β-TCP (PT) microspheres were performed using a two-stage emulsification method. Briefly, PLGA (1 g) and Span 80 (0.1 % w/v) were dissolved in dichloromethane (DCM; 20 mL), and β-TCP (200 mg) was added to the PLGA/DCM solution via homogenization (15,000 rpm) to form solid-oil (S/O) phase [31]. The S/O phase was then added to 10 mL of polyvinyl alcohol (PVA) aqueous solution (1 % w/v) containing Tween 60 (0.1 % w/v) and dispersed using a homogenizer (IKA Germany) to form the second stage of emulsification, known as the solid-oil-water (S/O/W) phase. Finally, the suspension was added dropwise to 200 mL of a PVA aqueous solution (1 % w/v) containing Tween 60 (0.1 % w/v) and continuously stirred at room temperature (300 rpm) for 6 h to allow for solvent evaporation. The solidified microspheres were collected, washed with deionized water, and freeze-dried. Further modification of the PLGA/β-TCP microspheres was achieved using poly-L-lysine (PLL) [32]. Specifically, the PLGA/β-TCP microspheres were first immersed in an excess of 0.1 M NaOH solution at room temperature for 30 min, followed by thorough washing with distilled water five times to remove any residual NaOH solution. The microspheres were then incubated overnight in 10 mL of a 0.25 % (wt/vol) PLL solution (deionized water) at 4 °C and subsequently washed with distilled water to remove any excess solution, yielding the PLL-PLGA (PP) and PLL-PLGA/β-TCP (PPT) microspheres, which were freeze-dried and stored at −20 °C before use. To encapsulate MM onto the PPT microspheres, MM was mixed with PPT in a mass ratio of membrane protein: PPT = 1:100 at 4 °C in DPBS to obtain and MM@PPT. The extraction temperature of the material infusion used in this experiment is (37 ± 1) °C, and the time is (72 ± 2) hours.

2.8. Characterization of microspheres

The morphology of the prepared microspheres was observed using a scanning electron microscope (SEM; JEOL JSM 7500F, Japan). Disperse 30 mg of microspheres in 10 mL PBS and shake in a constant temperature water bath at 37 °C (60 rpm). Replace the solution every 7 days. Collect microsphere at 7, 14 and 28 days for SEM observation of microsphere morphology. Weigh 3 mg of microspheres and 200 mg of potassium bromide (KBr) powder, then grind and mix them thoroughly. Use a pellet press to prepare a transparent pellet for testing. Set the infrared spectrometer to a wavenumber range of 400 cm^{-1} to 4000 cm^{-1} to obtain the FTIR spectrum. The cell membrane was stained using the Cell Plasma Membrane Staining Kit with DiI (Red Fluorescence) (Beyotime, China). The specific procedure was as follows: DiI, staining enhancer, and staining buffer were premixed in advance, added to the cell membrane, and incubated at 37 °C in the dark for 5 min, followed by centrifugation at 14,000 g for 30 min. The cell membrane staining working solution was then removed, and the membrane was washed 2–3 times with deionized water.

2.9. Cell viability

Bone Marrow Stem Cells (BMSCs) were seeded at a density of 2000 cells per well in a 96-well plate. The extracts from each group of microspheres were prepared, and the cells were cultured for 1, 3, 5, and 7 days to evaluate cell proliferation using the Cell Counting Kit-8 (Dojindo, Japan). The extract was removed, and the cells were washed with PBS. Then, 100 μL of fresh 10 % CCK-8 in α-MEM culture medium was added to each well and incubated at 37 °C for 1 h to measure the optical density (OD) values. Additionally, live/dead staining was performed on the cells cultured with the microsphere extracts after 1 and 3 days using a live/dead staining kit to assess the cytotoxicity of various microspheres.

2.10. Cell migration

To assess cell migration, this study employed both wound healing assay and Transwell assay. For the wound healing assay, BMSCs were cultured in a 6-well plate until they reached 90 % confluence. A wound approximately 1.5 mm wide was created using a blue pipette tip, and the cells were washed three times with PBS. The extracts of various groups of microspheres containing 2 % FBS were added to the wells, and the cells were incubated for an additional 24 h. The extent of wound healing was observed under an optical microscope and analyzed using ImageJ software.

For the Transwell assay, 200 μL of medium containing 5000 BMSCs were seeded in the upper chamber with an 8 μm pore filter membrane (Corning, America). The lower chamber was filled with 600 μL of various microsphere extracts containing 2 % FBS. After 24 h of incubation, the cells were washed three times with PBS, fixed with 4 % formaldehyde, and gently wiped with a cotton swab to remove non-migrated cells. The cells were then stained with 1 % crystal violet for 30 min. The relative number of migrated cells was counted and analyzed in five randomly selected microscopic fields on each membrane.

2.11. Immunomodulatory effects of MM@PPT microspheres on RAW264.7 cells

RAW264.7 cells were seeded in 6-well plates and confocal culture dishes and cultured in media containing LPS (100 ng/mL) for 24 h. The control group consisted of macrophages that were either untreated or treated with LPS. After discarding the supernatant, the cells were treated with extracts from each group of microspheres and cultured for an additional 3 days. The cells were then washed 3 times with PBS and fixed with 4 % paraformaldehyde at 4 °C for 30 min. Subsequently, the cells were permeabilized with 0.5 % Triton X-100 for 30 min and incubated with 5 % BSA for 1.5 h. The cells were then incubated with anti-inducible Nitric Oxide Synthase (iNOS) (1:50, Proteintech, China), anti-IL-1 (1:50, Abcam, UK), anti-CD206 (1:50, Proteintech, China) overnight at 4 °C. Afterwards, the macrophages were incubated with an Alexa Fluor 488 conjugate in the dark for 1 h. The cells were then incubated with DAPI containing an anti-fluorescence quencher for 30 min, and the intensity of green fluorescence was observed using a confocal microscope (Leica, Germany). ImageJ software was used for quantitative assessment. Total RNA was extracted from the cells in the 6-well plates and reverse transcribed into cDNA. qRT-PCR was then performed on the cDNA samples, and GAPDH was used as the reference gene. The primer sequences for IL-1 and CD206 are listed in Table S1. The experiment was repeated three times to ensure the accuracy of the results.

2.12. Indirect Co-culture system of BMSCs and RAW264.7 cells

2.12.1. Preparation of extracts

Microsphere-treated RAW264.7 cells-Conditional medium: RAW264.7 cells were seeded in 6-well plates and cultured in media containing LPS (100 ng/mL) for 24 h. The control group consisted of macrophages that were either untreated or treated with LPS. After discarding the supernatant, extracts from each group of microspheres were added, and the cells were cultured for an additional 3 days. The supernatant was collected and centrifuged at 3000 rpm for 10 min and then mixed with α-MEM in a 1:1 (volume ratio) to obtain the RAW264.7 cells-microsphere conditional medium. The corresponding extracts were named R-DMEM, R-PP, R-PPT, and R-MM@PPT.

Microsphere-treated BMSCs Conditional medium: BMSCs were seeded in 6-well plates, and extracts from each group of microspheres

were added. The control group consisted of BMSCs cultured in a regular medium. The supernatant was collected on days 5–7 and centrifuged at 3000 rpm for 10 min to obtain the supernatant. This supernatant was mixed with fresh DMEM in a 1:1 ratio to generate the BMSCs-microsphere conditional medium. The corresponding extracts were named B-MEM, B-PP, B-PPT, and B-MM@PPT.

2.12.2. Immunomodulatory effects of microsphere-treated BMSCs conditional medium on RAW264.7 cells

RAW264.7 cells (1×10^5 cells per well) were seeded in 6-well plates and treated with LPS (100 ng/mL) for 24 h before switching to the BMSCs-microsphere conditional medium. RAW264.7 cells cultured without LPS induction in standard culture medium served as a negative control (B-Control), while RAW264.7 cells in B-MEM medium that were LPS-induced served as a positive control (B-MEM + LPS). The specific experimental groups included B-MEM, B-MEM + LPS, B-PP + LPS, B-PPT + LPS, and B-MM@PPT + LPS. After 3 days of culture, RT-qPCR was performed to detect the expression of macrophage polarization-related genes (IL-1, CD206).

For immunofluorescence staining, RAW264.7 cells (5×10^4 cells per well) were seeded in laser confocal culture dishes. After 3 days of culture, the cells were washed, fixed, permeabilized, and blocked, followed by co-incubation with antibodies anti-iNOS (1:50, Proteintech, China), anti IL-1 (Abcam, UK) and anti-CD206 (Proteintech, China). Confocal laser scanning microscopy (CLSM) was used for imaging, and ImageJ was utilized to analyze fluorescence intensity. Total RNA was extracted from the cells in the 6-well plates and reverse transcribed into cDNA. RT-qPCR was then conducted on the cDNA samples, with GAPDH used as the reference gene, to measure the expression levels of IL-1 and CD206.

2.12.3. Regulation of BMSCs osteogenic differentiation by microsphere-treated RAW264.7 cells-conditional medium

BMSCs (5×10^4 cells per well) were seeded in 24-well plates, and different osteogenic extracts were added: R-DMEM, R-DMEM + LPS, R-PPT + LPS, and R-MM@PPT + LPS. After 7 and 14 days, alkaline phosphatase (ALP) staining, Alizarin Red S (ARS) staining, and RT-qPCR analysis were performed, with the primer sequences listed in Table S2. The experiments were repeated three times to ensure the accuracy of the results, and the relative quantification of gene expression was calculated using the 2^(-ΔΔCt) method.

2.12.4. Inhibition of osteoclast activation by microsphere-treated BMSCs conditional medium

BMSCs were seeded in 6-well plates, and RANKL (100 ng/mL) was added to the microsphere extracts. The MEM group without RANKL served as the negative control, while the MEM + RANKL (100 ng/mL) group served as the positive control. The specific experimental groups included B-MEM, B-MEM + RANKL, B-PP + RANKL, B-PPT + RANKL, and B-MM@PPT + RANKL. RAW264.7 cells (3×10^4 cells) were seeded in 6-well plates and co-cultured with the aforementioned extracts for 4 days. RT-qPCR was performed to assess the expression levels of osteoclast-related genes (Cathepsin K, TRAP, and MMP9). The primer sequences are listed in Table S3. Additionally, TRITC-labeled phalloidin/DAPI staining was used to observe cell morphology, and images were taken using a confocal laser scanning microscope (CLSM). Fix the cells with TRAP fixative at 4 °C for 30 s to 3 min. After washing with PBS, incubate them in TRAP staining solution and place them in a 37 °C incubator for 45–60 min under light-protected conditions. Subsequently, stain the samples with hematoxylin for 3–5 min, followed by bluing with tap water.

2.13. Rat periodontitis model

The animal experiments were approved by the Animal Use and Management Committee of Peking University (LA2024075), and all procedures complied with institutional animal use guidelines. Twelve male Sprague-Dawley rats (5 weeks old, weighing 180–220 g) were acclimatized in a controlled environment for 1 week and then randomly divided into four groups: 1) PBS Control Group: Treated with PBS, 2) PP Group: Treated with PLL-PLGA (PP) microsphere, 3) PPT Group: Treated with PLL-PLGA/TCP (PPT) microspheres for periodontitis, 4) MM@PPT Group: Treated with macrophage membrane vesicle-functionalized PLL-PLGA/TCP (MM@PPT) microspheres.

The rats were anesthetized with isoflurane inhalation, and a 2.0 mm ligature wire was securely tied around the cervical region of the maxillary first molar (M1) using a needle holder. The ligature was checked every 4 days, and LPS (1 mg/mL, 20 μL) was injected into the palatal gingiva between the first and second molars every 3 days. After 4 weeks, the ligature was removed, and microspheres (10 mg/kg) were injected into the defect site. At 4 weeks post-surgery, the rats were euthanized, and the maxillae were fixed in 10 % neutral buffered formalin. Imaging was performed using Micro-CT, and both 2D and 3D reconstruction was performed to analyze the distance from the cementoenamel junction to the alveolar bone crest (CEJ-ABC) and bone volume fraction (BV/TV). The samples were embedded and sliced. H&E staining, Masson staining, and TRAP staining were conducted to evaluate bone tissue formation in the regenerated tissue. Immunohistochemical staining was performed to analyze the expression of OPN and IL-6 in the slice samples.

2.14. Statistical analysis

Data were collected and analyzed using SPSS 27.0 software. All quantitative data are expressed as mean ± standard deviation (SD), with a sample size of ($n \geq 3$). Statistical analyses were performed using one-way or two-way analysis of variance (ANOVA), followed by Tukey's analysis. A significance level of $^*p < 0.05$ was considered statistically significant, while $^{**}p < 0.01$, $^{***}p < 0.001$, and $^{****}p < 0.0001$ were considered highly significant differences.

3. Results and discussion

3.1. Design and preparation of MM@PPT microspheres

According to previous reports, M1 macrophages express more inflammatory factor receptors than M0 and M2 macrophages [12]. Therefore, we extracted membrane vesicles from macrophages with higher cytokine receptor expression levels under two different stimulation methods (LPS and LPS + IFN-γ), and the membrane vesicles with the highest cytokine receptor expression was selected to coat PLL modified PLGA (PP) and PLGA/β-TCP (PPT) microspheres (Fig. 1A). All three types of macrophage membrane vesicles (MM) were spherical (Fig. 1B), while DLS revealed similar size distributions for the three types of vesicles (Control: 172.85 nm, LPS: 148.58 nm, LPS + IFN-γ: 216.36 nm) (Fig. 1C), with zeta potentials of −6.51 mV, −11.96 mV, and −10.79 mV, respectively (Fig. 1D).

The receptors on the macrophage membrane surface are key components in neutralizing inflammatory factors such as IL-6 and TNF-α, which lead to severe periodontal inflammation and alveolar bone resorption [33,34]. First, we performed Western blotting and flow cytometry, and the results showed that under stimulation with LPS + IFN-γ, the macrophage membrane had higher levels of TNF-αR and IL-6R compared to the LPS and control groups (Fig. 1E–G). To further validate the ability of various macrophage membrane vesicles to neutralize pro-inflammatory cytokines, we added different concentrations of macrophage membrane vesicles (10, 50, 100, and 500 μg/mL) to solutions containing TNF-α or IL-6 and incubated them. The ability of these MM in neutralizing TNF-α and IL-6 showed a concentration-dependent manner, and similar to the levels of TNF-αR and IL-6R, LPS + IFN-γ group has a stronger ability to neutralize inflammatory factors and can remove all the inflammatory factors in 500 μg/mL (Figs. S1 and S2).

The SEM images show that the PPT microspheres are spherical in

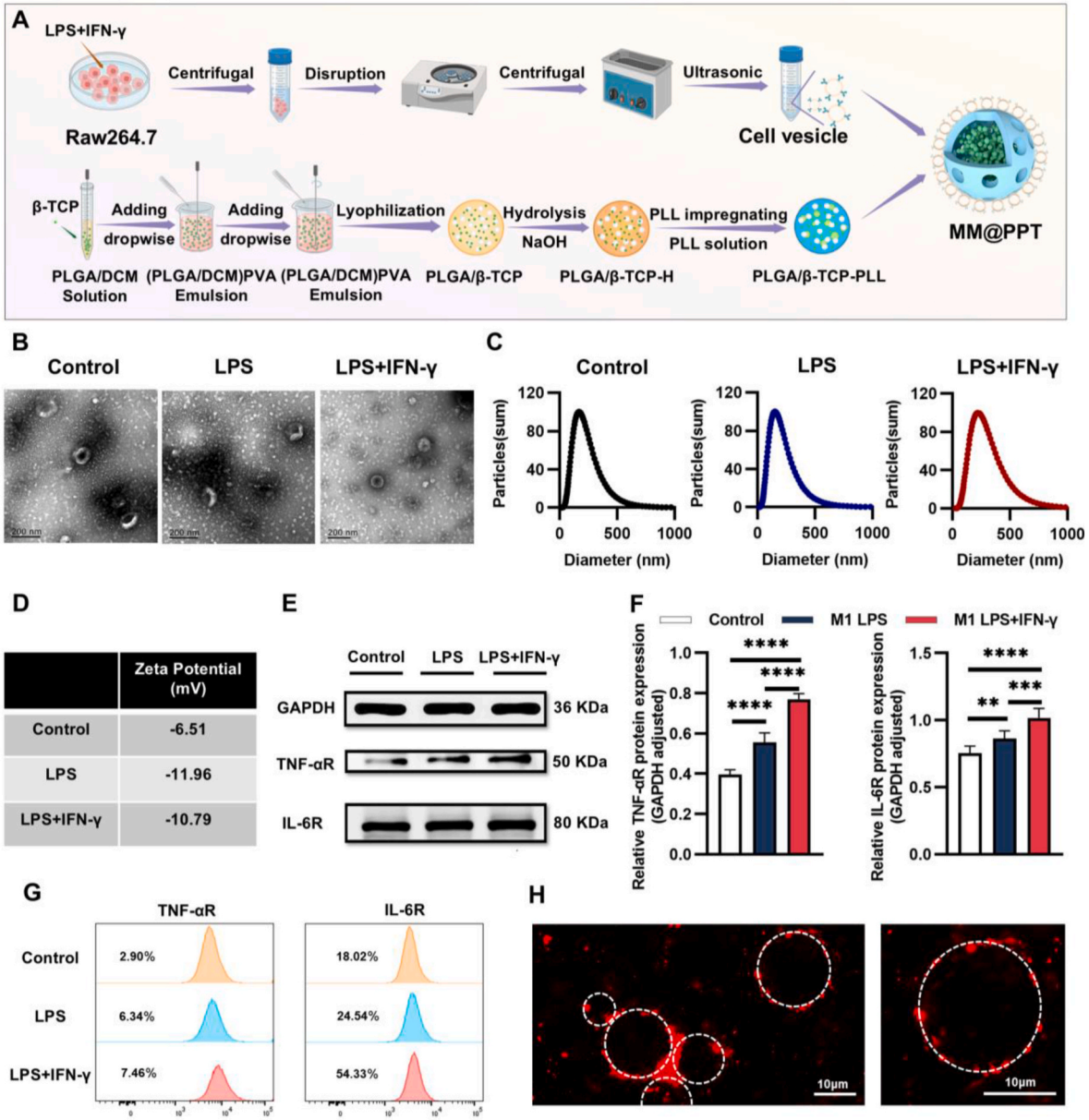

Fig. 1. Characteristics of macrophage membrane vesicles (MM) and MM@PPT. (A) Schematic diagram of the preparation process of MM@PPT.(B) Morphology of MM observed by transmission electron microscopy (TEM). (Scale bar = 200 nm) (C) NTA analysis of MM and (D) zeta potential analysis. The expression of TNFα-R and IL-6R on macrophages treated with 100 ng/mL LPS and 100 ng/mL LPS +10 ng/mL IFN-γ was evaluated by (E) Western blot, (F) corresponding quantitative results analyzed by ImageJ ($n \geq 3$), and (G) flow cytometry histogram. (H) Fluorescence staining of macrophage membrane vesicle-functionalized PPT observed under CLSM. PPT: white circle, MM: red. (Scale bar: 10 μm) ($n \geq 3$) *$p < 0.05$, **$p < 0.01$, ***$p < 0.001$, ****$p < 0.0001$. (For interpretation of the references to colour in this figure legend, the reader is referred to the Web version of this article.)

shape with an average diameter of ~15 μm (Fig. S3). Fom 1–4 weeks of degradation, the surfaces of all groups of microspheres became increasingly porous, gradually forming collapsed large-pore structures. During this process, the particle size of all types of microspheres also gradually decreased with prolonged soaking time. After 28 days of degradation, all microspheres were still able to maintain their spherical structure (Fig. S4). Poly-L-lysine (PLL) is commonly used as a coating to enhance cell adhesion in standard cell culture processes, which is based on the interaction between the positively charged PLL and negatively charged cell membrane [29,32]. Here, after PLL modification, which allows binding to negatively charged macrophage membrane through electrostatic interaction, enabling the macrophage membrane binding to microspheres. The FT-IR spectra demonstrated the successful modification of PLL. Both PT microspheres and PPT microspheres exhibited characteristic PLGA peaks around 1750 cm^{-1} (C=O group) and 1260 cm^{-1} (C–O–C group). In contrast, the PPT microspheres displayed a new peak around 1540 cm^{-1}, corresponding to the N–H deformation vibration peak (Amide II) of PLL molecules (Fig. S5). To evaluate the distribution of MM on PPT, we labeled MM with red fluorescence. The MM (red) coating on the PPT remained stable, and the microspheres showed a uniform distribution of MM (Fig. 1H). MM@PPT mimics the size of macrophages and effectively replicates the critical receptors for neutralizing inflammatory factors derived from the source macrophages, expected to serve as an effective tool for neutralizing inflammatory factors to regulate the inflammatory microenvironment in periodontal tissues.

3.2. In vitro promotion of the osteogenesis of BMSCs by MM@PPT

The extracted BMSCs were identified with typical morphology and specific markers (e.g., CD29 and CD90) (Figs. S6 and S7). To evaluate the effect of MM@PPT on the viability, migration, and osteogenesis of BMSCs, we collected extracts from different microspheres (PP, PPT, and MM@PPT) (Fig. 2A). The CCK-8 assay measured the proliferation of BMSCs in different extracts. From day 1 to day 7, the cells continued to proliferate under different extracts, with the MM@PPT group displaying a significantly enhanced proliferation capacity compared to the other three groups (Fig. 2B). In the meantime, live/dead staining demonstrated a large number of living cells (green) under the various extracts (Fig. 2C and S8), indicating excellent cell compatibility for PP, PPT, and MM@PPT microspheres. Moreover, the morphology of cells in extracts remained spindle-shaped in all groups (Fig. S9).

Repairing alveolar bone in periodontitis, especially for in situ bone regeneration, requires the homing of endogenous cells, which can further promote tissue remodelling [35–37]. We used wound healing and Transwell assays (Fig. 2D and E) to evaluate the migration capability of BMSCs. The standardised repair area in the MM@PPT group was 84.38 %, with 129 migrating cells per field of view, which was 1.3 times and 2.4 times higher than the Control group, 1.2 times and 2.1 times higher than the PP group, and 1.8 times and 1.1 times higher than the PPT group, respectively. This indicates that MM@PPT significantly promotes stem cell migration both horizontally and vertically.

To investigate the effects of MM@PPT on the osteogenesis of BMSCs, cells were cultured in osteogenic media (OM) containing different microsphere extracts for 7 and 14 days, followed by ALP, ARS staining (Fig. 2F) and semi-quantitative analysis (Fig. S10). The ALP and ARS staining are upregulated in the order of PP < PPT < MM@PPT.

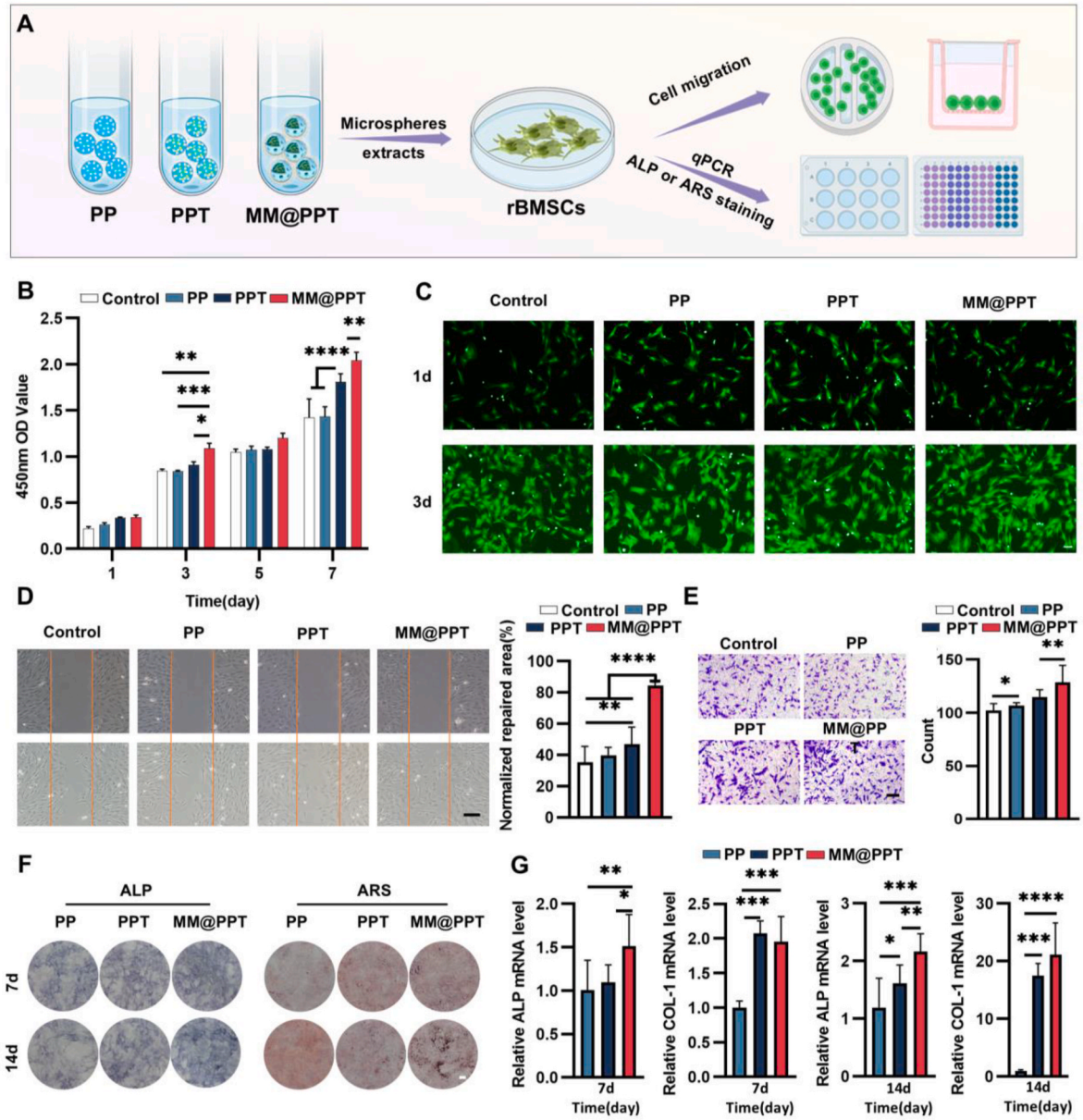

Fig. 2. MM@PPT promotes the proliferation, migration, and osteogenic differentiation of BMSCs. (A) A schematic diagram illustrates the extraction of material extracts used to study osteogenesis. (B) Quantitative assessment of proliferation capacity through CCK8 test on days 1, 3, 5, and 7. (C) Observation of cell viability using optical microscopy (OM) and live/dead staining. (Scale bar: 500 μm) (D) Wound healing assay for BMSCs migration (Scale bar: 500 μm) and corresponding quantitative analysis. (E) Transwell assay for BMSCs cell migration (Scale bar: 200 μm) and corresponding quantitative analysis. (F) ALP and ARS staining (Scale bar: 200 μm). (G) Expression of osteogenic genes (ALP, COL-1) in BMSCs on days 7 and 14. ($n \geq 3$) *p < 0.05, **p < 0.01, ***p < 0.001, ****p < 0.0001.

MM@PPT induced high expression levels of osteogenesis-related genes (ALP and COL-I) (Fig. 2G). RT-qPCR results demonstrate that the expression level of ALP is 1.5 times and 1.8 times higher at 7 days and 14 days in the MM@PPT group compared to the PP group and 1.4 times and 1.3 times higher compared to the PPT group. The expression level of COL-1 is 1.9 times and 21.1 times higher compared to the PP group. Although at 7 days, the COL-1 expression in the MM@PPT group shows no difference compared to the PPT group, it is 1.2 times higher at 14 days. ALP and COL-1 protein expression results are similar to RT-qPCR (Fig. S11). The ability of MM@PPT to promote cell migration and osteogenic differentiation can be attributed to two main factors: firstly, the β-TCP contained in MM@PPT can release Ca^{2+} and PO_4^{3-}, thereby enhancing osteogenesis as reported in our previous work [27]; secondly, besides inflammatory factor receptors, MM also possesses various osteogenic ligands, such as Annexin A1 (ANXA1) and chemokine receptor CCR2 [38,39].

3.3. *In vitro reversal of the inflammatory microenvironment by MM@PPT*

Due to the pro-inflammatory nature of macrophages in the pathogenesis of periodontitis, their role in the progression of the disease has garnered considerable attention [40]. To assess the regulatory effects of MM@PPT on the phenotype and function of pro-inflammatory macrophages, we first polarized macrophages to the M1 phenotype and then treated them with various microsphere extracts. We analyzed the expression of representative proteins/genes related to inflammatory regulation in macrophages (Fig. 3A). Macrophages stimulated with LPS appeared flattened with dispersed cell distribution and numerous pseudopodia (Fig. 3B). In contrast, macrophages cultured with various extracts gradually transitioned from pseudopod-like structures and elongated phenotype to a round morphology with fewer surface protrusions, indicating polarization towards an M2 phenotype. Similarly, macrophages in DMEM + LPS exhibited the strongest green fluorescence staining for iNOS and IL-1, while staining for CD206 was mainly negative, indicating M1 macrophage activation, followed by the PP group. In contrast, the MM@PPT group showed a more pronounced expression of CD206, followed by the PPT group, indicating enhanced M2 macrophage activation (Fig. 3C and D and S12). At the genetic level (Fig. 3E), MM@PPT group also displayed the most down-regulated pro-inflammatory iNOS and IL-1 gene expression and up-regulated anti-inflammatory CD206 gene expression, followed by the PPT group and PP group. These results revealed that the MM@PPT group had the strongest regulatory effect on the polarization of macrophages to the M2 phenotype in the inflammatory environment due the synergistic effect of MM (LPS + IFN-γ) and PTT microspheres. MM@PPT promotes M2 macrophage polarization primarily by neutralizing pro-inflammatory cytokines on the macrophage membrane and releasing Ca^{2+} through PPT

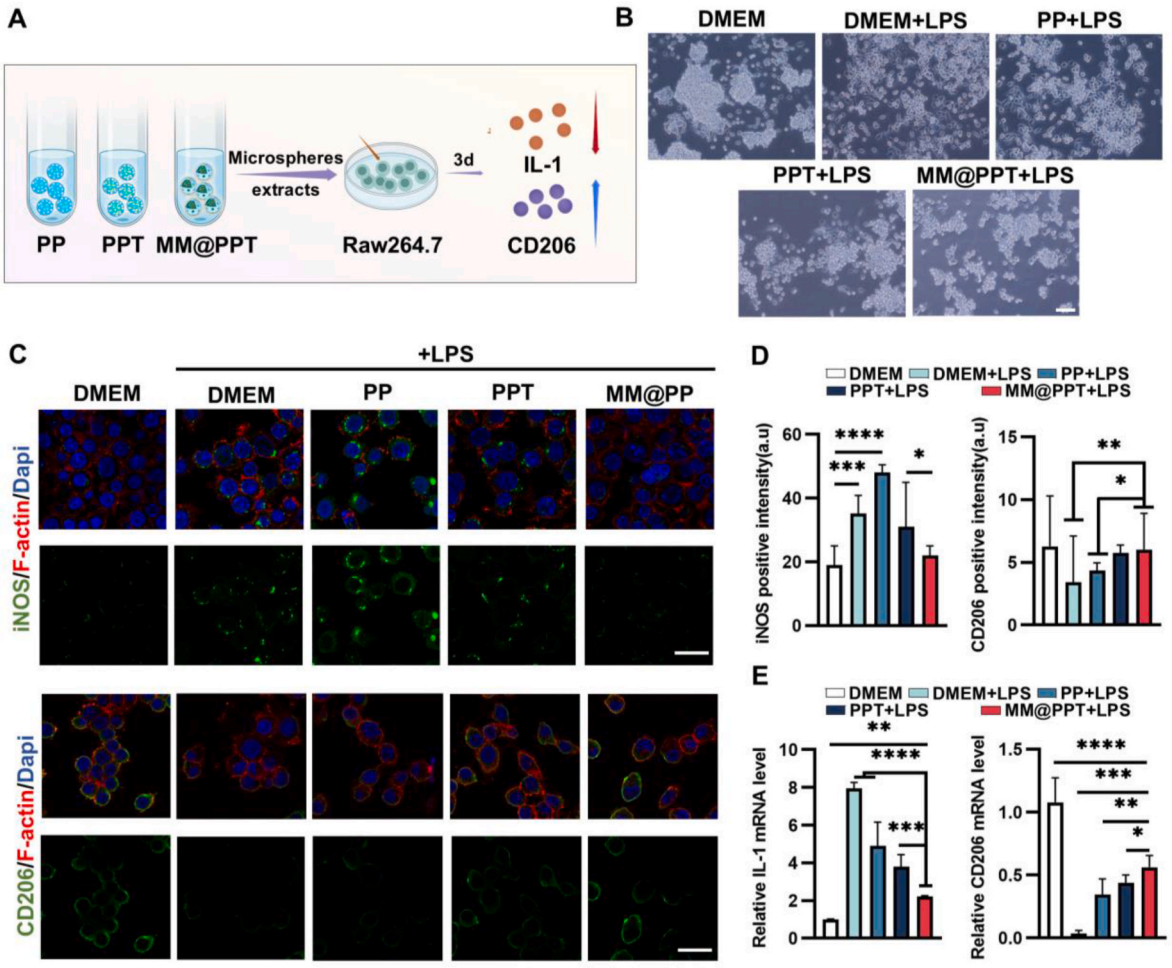

Fig. 3. Effect of MM@PPT on the polarization of RAW264.7 cells. (A) Schematic diagram of cell culture. Macrophages stimulated with LPS were cultured in microsphere extract for 3 days. (B) Morphology of RAW264.7 cells was observed under a light microscope after 3 days. (Scale bar: 200 μm) (C) CLSM image of iNOS and CD206 expression in RAW264.7 cells after 3 days. (Scale bar: 25 μm) (D) Quantitative analysis of the immunofluorescence staining intensity of M1 and M2 marker-positive macrophages. (E) mRNA expression levels of IL-1 and CD206 in RAW264.7 cells after 3 days. ($n \geq 3$) *$p < 0.05$, **$p < 0.01$, ***$p < 0.001$, ****$p < 0.0001$.

degradation. Specifically, PPT releases β-TCP which increases Ca^{2+} concentration in the extraction medium [41]. As a key signaling molecule, Ca^{2+} participates in various inflammatory pathways. Notably, Ca^{2+} can activate the CaSR signaling cascade to promote Wnt5A production, which exerts anti-inflammatory effects through dual mechanisms: (1) suppressing TNFα expression via NF-κB inhibition, and (2) downregulating TNFR1 through the Wnt5a/Ror2 pathway. These coordinated actions collectively promote macrophage polarization towards the M2 phenotype [42].

3.4. MM@PPT regulating osteogenesis-immunomodulation coupling via cross-culture

The scaffold materials in bone defect sites allow immune cells and BMSCs to work together, regulating the inflammatory microenvironment while creating a favorable microenvironment for tissue regeneration [43–45]. Therefore, we utilized an BMSCs-RAW264.7 cells-microsphere cross-culture system to investigate the regulatory effects of MM@PPT on the crosstalk between macrophages and BMSCs.

First, we assessed the impact of the conditional medium of microsphere extracts treated-BMSCs on LPS stimulated macrophages. In the MM@PPT + LPS group, we observed a decrease in iNOS and IL-1 fluorescence intensity and an increase in CD206 fluorescence intensity, confirming that MM@PPT promotes macrophage polarization towards the M2 phenotype. (Fig. 4B and C and S13). The IL-1 mRNA expression in the MM@PPT + LPS group was 3.25 times lower than the positive control, while the CD206 mRNA expression was 2.14 times higher than that of the positive control (Fig. 4D). These compelling results suggest that MM@PPT can cooperate with BMSCs to inhibit the M1 phenotype

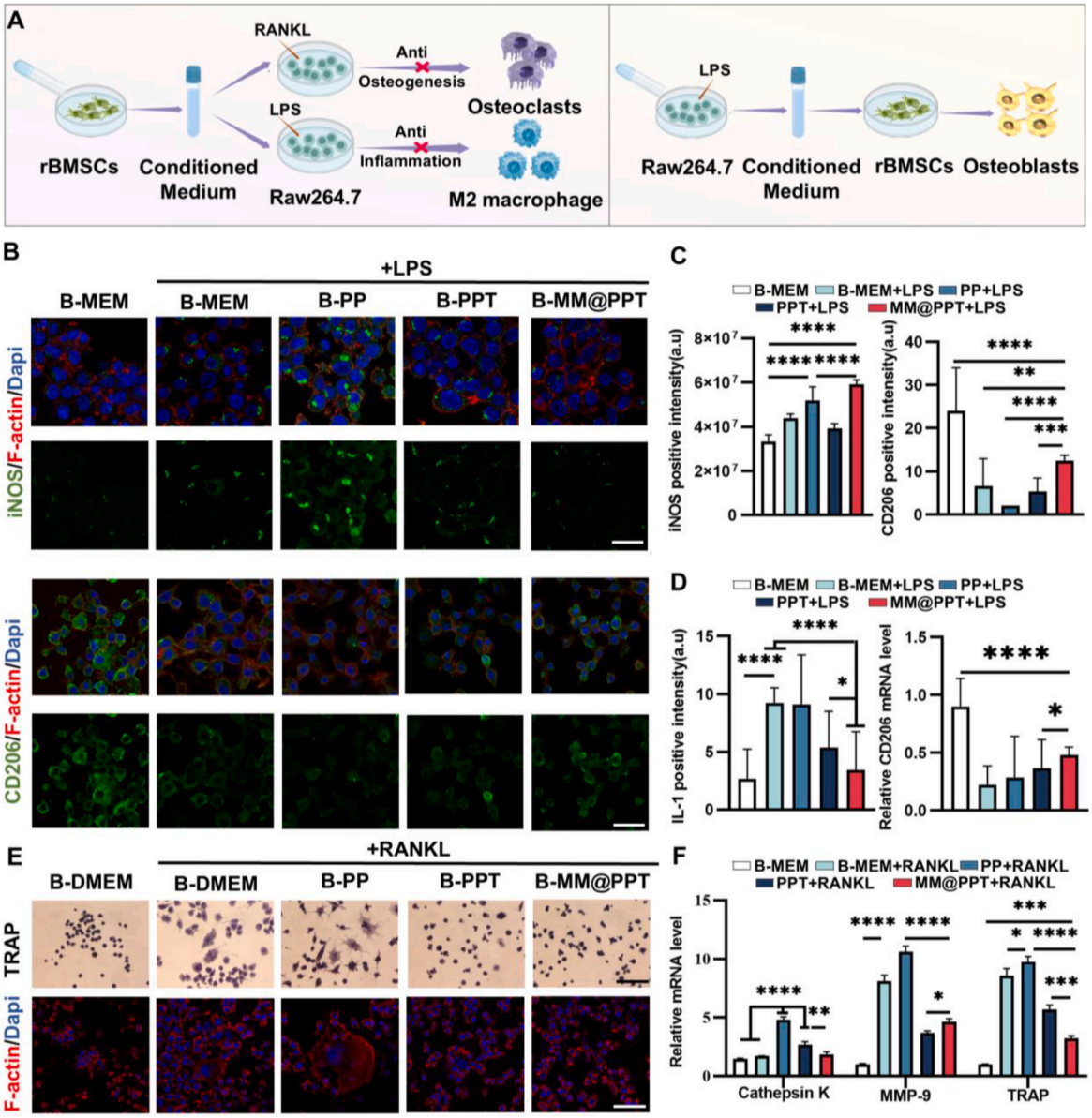

Fig. 4. Osteoclast-immune regulatory coupling in the indirect co-culture system of BMSCs and RAW264.7 cells induced by MM@PPT. (A) Schematic diagram of cell culture. It shows the effect of BMSCs-microsphere conditional medium on the polarization and osteoclast differentiation of RAW264.7 cells. (B–E) Effects of BMSCs-microsphere conditional medium on the polarization of RAW264.7 cells: (B) CLSM image of iNOS and CD206 in RAW264.7 cells after 3 days. (Scale bar: 25 μm) (C) Quantitative analysis of the immunofluorescence staining intensity of M1 and M2 marker-positive macrophages. (D) mRNA expression levels of IL-1 and CD206 in RAW264.7 cells after 3 days. (E–F) Effects of BMSCs-microsphere conditional medium on the osteoclast differentiation of RAW264.7 cells: (E) CLSM image of F-actin in RAW264.7 cells. (Scale bar: 50 μm) (F) RT-qPCR analysis of osteoclast-related gene expression. ($n \geq 3$) *$p < 0.05$, **$p < 0.01$, ***$p < 0.001$, ****$p < 0.0001$.

and effectively promote M2 polarization.

The effects of MM@PPT-mediated RAW264.7 cells on BMSC osteogenic response were further investigated. ALP and ARS staining, as well as RT-qPCR, were performed on days 7 and 14 (Figs. S14–S17). The results showed that the conditional medium LPS-stimulated RAW264.7 cells significantly inhibited the osteogenesis of BMSCs. However, upon introducing the RAW264.7 cells-microsphere conditional medium, higher expression levels of osteogenesis-related genes (RUNX2, BMP-2, OPN, and ALP) can be detected. These results indicate that MM@PPT facilitates the collaborative role of macrophages and BMSCs in promoting tissue regeneration in the inflammatory microenvironment.

Maintaining bone tissue homeostasis requires the collaborative action of osteoblasts and osteoclasts, and osteoclasts are over-activated in periodontitis. [46,47]. The extracted microsphere supernatant was co-cultured with BMSCs and RAW264.7 cells under RANKL stimulation. Immunofluorescence staining and tartrate resistant acid phosphatase (TRAP) staing revealed that mature osteoclasts exhibited a multinucleated morphology. B-PP group promote osteoclast differentiation. The promotion of osteoclast formation in the B-PP group is primarily associated with the acidic degradation products of PLGA. PLGA is a biodegradable aliphatic amorphous polymer synthesized through the copolymerization of two monomers: lactic acid (LA) and glycolic acid (GA) [48]. The acidic degradation products of its monomers and oligomers can reduce the local pH both within the scaffold and surrounding the implantation site. Compared to the positive control group (B-Control + RANKL), the MM@PPT group displayed the least number of TRAP-positive multinucleated cells (Fig. 4E), significantly reduced expression levels of TRAP, matrix metalloproteinase 9 (MMP9), and Cathepsin K (Fig. 4F). The B-PPT + RANKL group showed slightly less inhibitory effect on osteoclast maturation compared to the MM@PPT + RANKL group. Collectively, MM@PPT can inhibit M1 macrophage polarization and osteoclast differentiation, favor their polarization to M2, and enhance the osteogenic differentiation potential of BMSCs, thus improving the bone immune microenvironment.

3.5. *MM@PPT promotes alveolar bone regeneration in a ligature-induced rat periodontitis model*

The scaffold materials in bone defect sites allow immune cells and BMSCs to work together, regulating the inflammatory microenvironment while creating a favorable microenvironment for tissue regeneration [7,49–51]. Therefore, we utilized a BMSCs-RAW264.7 cells-microsphere cross-culture system to investigate the regulatory effects of MM@PPT on the crosstalk between macrophages and BMSCs.

In view of the effective role of MM@PPT in regulating macrophages and BMSCs, we established a rat periodontitis animal model to investigate the *in vivo* effects of MM@PPT on alveolar bone resorption in periodontitis. Four weeks post-ligation, we injected PBS, PP, PPT, and MM@PPT microspheres into the periodontal pockets. Micro-CT analysis was performed to generate 3D and 2D reconstructed images (Fig. 5B),

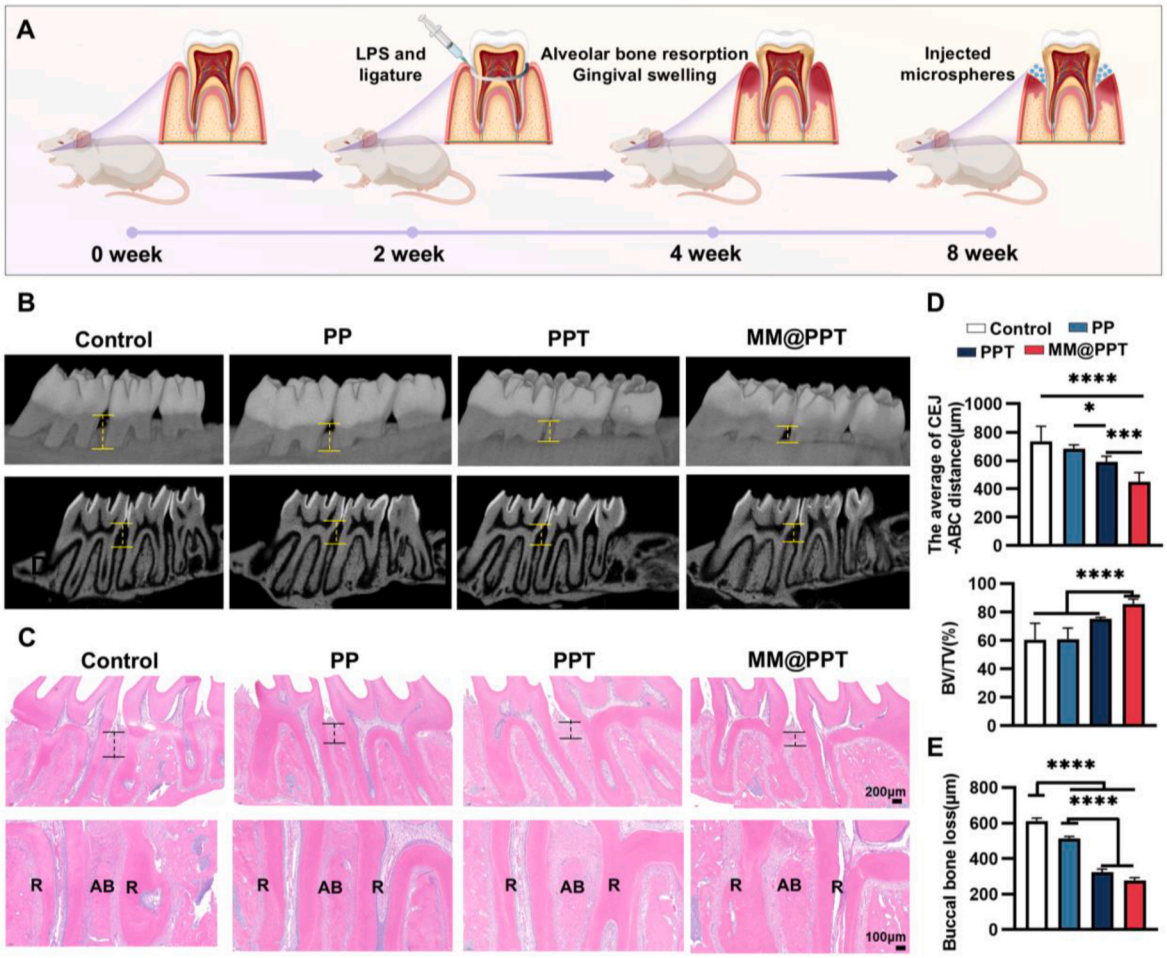

Fig. 5. Assessment of bone regeneration *in vivo* after 4 weeks of microsphere treatment. (A) Schematic diagram of the maxillary alveolar bone in periodontitis and three microsphere treatment groups. (B) 3D reconstruction and 2D images after 4 weeks of implantation. (C) H&E staining images (D) CEJ-ABC distance and BV/TV values. (E) Corresponding buccal bone loss measurement of the maxilla in the control group and the three microsphere treatment groups. *p < 0.05, **p < 0.01, ***p < 0.001, ****p < 0.0001.

followed by quantitative analysis of new bone tissue using BV/TV, cementoenamel junction (CEJ)-alveolar crest (ABC) measurements and buccal bone loss. The periodontitis control group showed significant alveolar bone resorption and root exposure. In contrast, the PPT and MM@PPT groups exhibited higher alveolar bone levels. The 2D images further confirmed this trend. Additionally, the CEJ-ABC distance measured in the 2D images to assess vertical bone resorption was consistent with the findings from the 3D images. The CEJ-ABC distance in the PPT and MM@PPT groups was smaller compared to the control group. The 3D reconstruction of alveolar bone between the first and second molars revealed that the BV/TV values in the MM@PPT group was 85.27 %, which was significantly higher than that in the control (60.49 %), PP(60.96 %), and PPT (75.08 %) groups (Fig. 5D).

We performed H&E staining to elucidate the histological

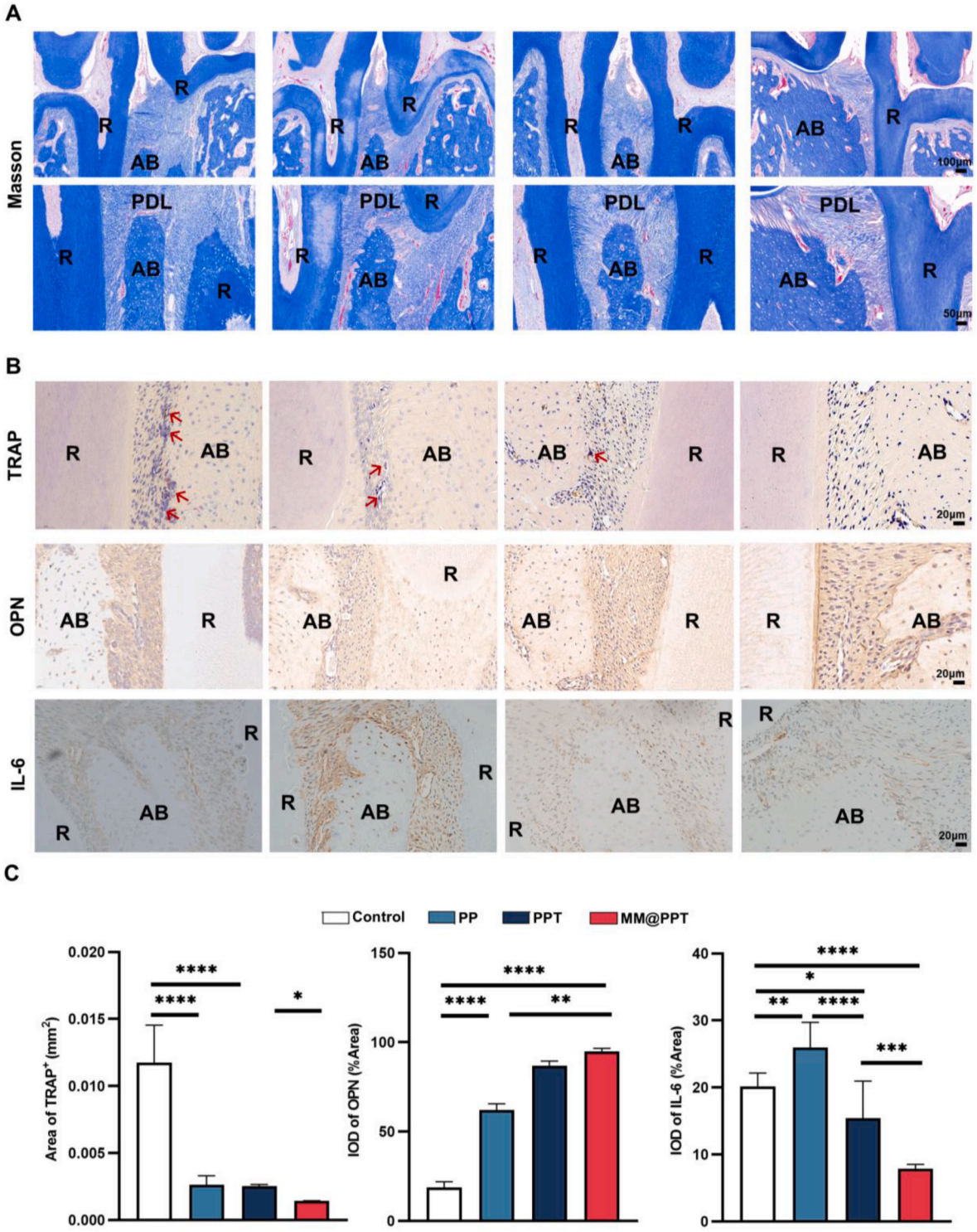

Fig. 6. Histological analysis of bone regeneration *in vivo* after 4 weeks of microsphere treatment (A) Masson staining. (B) Representative immunohistochemical staining image of TRAP, OPN and IL-6 (TRAP-positive cells indicated by red arrows). (C) Semiquantitative statistics of TRAP, OPN and IL-6. R: root, AB: alveolar bone, PDL: periodontal ligament. (For interpretation of the references to colour in this figure legend, the reader is referred to the Web version of this article.)

morphology of the alveolar bone (Fig. 5C and E). The results from H&E staining indicated a significant reduction in alveolar bone height in the control group. In contrast, both the PPT and MM@PPT groups showed repaired alveolar bone compared to the control group, with the MM@PPT group demonstrating notably higher alveolar bone levels than the other three groups. Moreover, the arrangement of collagen fibres between the reconstructed alveolar bone and cementum appeared more densely packed and organized. The alveolar bone loss height in the MM@PPT group (277.9 μm) is lower than that in the control group (611.5 μm), PP group (513.7 μm), and PPT group (323.7 μm).

Masson staining indicated severe degradation of collagen fibres and tissues in the control group due to inflammatory damage at week 4 (Fig. 6A). The PPT and MM@PPT groups displayed nearly complete blue-stained collagen fibres, with the majority of newly formed alveolar bone being mature bone tissue. In addition, TRAP staining revealed a lower number of TRAP-positive cells in the MM@PPT group compared to the untreated group. To confirm the bone regenerative effect of the MM@PPT group, we performed immunohistochemical staining for the bone formation marker OPN. The PPT and MM@PPT groups exhibited higher expression and a larger area of deep staining compared to the control and PP groups. Immunohistochemical staining for IL-6 revealed that the PPT group and the MM@PPT group exhibited lower levels of IL-6 positive expression compared to the periodontitis control group and the PP group (Fig. 6B and C). These results suggest that MM@PPT enhances osteoblast activity while inhibiting osteoclast activation, synergistically improving alveolar bone tissue resorption in periodontitis.

4. Conclusion

In summary, we report the use of macrophage membrane functionalized PLGA/β-TCP microspheres for inflammation modulation and enhancement of endogenous bone regeneration in a rat periodontitis model. We found that macrophage membranes stimulated by LPS and IFN-γ can effectively neutralize inflammatory factors. The MM@PPT microspheres have the capacity to regulate cellular responses through various coupling effects, including inhibiting M1 polarization and osteoclast differentiation, favoring their polarization to M2, and enhancing the osteogenic differentiation potential of BMSCs even in an inflammatory microenvironment. Overall, this study not only provides MM@PPT microspheres for promoting alveolar bone regeneration in periodontitis but also investigates how these microspheres participate in regulating cell behavior and interactions. These results offer diverse therapeutic approaches for more effective alveolar bone repair.

CRediT authorship contribution statement

Rui Song: Writing – original draft, Project administration, Methodology, Investigation, Formal analysis, Data curation, Conceptualization. **Zhuo Wan:** Writing – original draft, Project administration, Methodology, Investigation, Formal analysis, Data curation, Conceptualization. **Xiaojing Yuan:** Writing – review & editing, Supervision, Resources, Project administration, Methodology, Funding acquisition, Conceptualization. **Nan Wang:** Visualization, Software, Methodology, Funding acquisition, Formal analysis. **Yike Gao:** Visualization, Software, Methodology, Formal analysis, Data curation. **Linxue Zhang:** Visualization, Software, Methodology, Formal analysis, Data curation. **Huihui Ren:** Visualization, Software, Methodology, Formal analysis, Data curation. **Yu Jin:** Validation, Resources, Methodology, Data curation. **Xiya Liu:** Validation, Resources, Methodology, Data curation. **Jingyi Sang:** Validation, Resources, Methodology, Data curation. **Zuoying Yuan:** Writing – review & editing, Supervision, Resources, Project administration, Methodology, Funding acquisition, Conceptualization. **Yuming Zhao:** Writing – review & editing, Supervision, Resources, Project administration, Methodology, Funding acquisition, Conceptualization.

Declaration of competing interest

The authors declare that they have no known competing financial interests or personal relationships that could have appeared to influence the work reported in this paper.

Acknowledgments

This work was supported by National Natural Science Foundation of China (Grant no. 82201019), Natural Science Foundation of Beijing Municipality (Grant no. L242158, L222144, L246035, 7244516), and the China Postdoctoral Science Foundation funded project (Grant no.2024M750112)

Appendix A. Supplementary data

Supplementary data to this article can be found online at https://doi.org/10.1016/j.mtbio.2025.101789.

Data availability

Data will be made available on request.

References

[1] B.L. Pihlstrom, B.S. Michalowicz, N.W. Johnson, Periodontal diseases, Lancet (London, England) 366 (9499) (2005) 1809–1820.
[2] D.F. Kinane, P.G. Stathopoulou, P.N. Papapanou, Periodontal diseases, Nat. Rev. Dis. Primers 3 (2017) 17038.
[3] H. Hasturk, A. Kantarci, Activation and resolution of periodontal inflammation and its systemic impact, Periodontology 69 (1) (2000 2015) 255–273.
[4] T.E. Van Dyke, C. Sima, Understanding resolution of inflammation in periodontal diseases: is chronic inflammatory periodontitis a failure to resolve? Periodontology 82 (1) (2000 2020) 205–213.
[5] F. Graziani, D. Karapetsa, B. Alonso, D. Herrera, Nonsurgical and surgical treatment of periodontitis: how many options for one disease? Periodontology 75 (1) (2000 2017) 152–188.
[6] X. Ji, X. Yuan, L. Ma, B. Bi, H. Zhu, Z. Lei, W. Liu, H. Pu, J. Jiang, X. Jiang, Y. Zhang, J. Xiao, Mesenchymal stem cell-loaded thermosensitive hydroxypropyl chitin hydrogel combined with a three-dimensional-printed poly(ε-caprolactone)/nano-hydroxyapatite scaffold to repair bone defects via osteogenesis, angiogenesis and immunomodulation, Theranostics 10 (2) (2020) 725–740.
[7] S. Yang, Y. Zhu, C. Ji, H. Zhu, A. Lao, R. Zhao, Y. Hu, Y. Zhou, J. Zhou, K. Lin, Y. Xu, A five-in-one novel MOF-modified injectable hydrogel with thermo-sensitive and adhesive properties for promoting alveolar bone repair in periodontitis: antibacterial, hemostasis, immune reprogramming, pro-osteo-/angiogenesis and recruitment, Bioact. Mater. 41 (2024) 239–256.
[8] W. Wang, C. Zheng, J. Yang, B. Li, Intersection between macrophages and periodontal pathogens in periodontitis, J. Leukoc. Biol. 110 (3) (2021) 577–583.
[9] X. Sun, J. Gao, X. Meng, X. Lu, L. Zhang, R. Chen, Polarized macrophages in periodontitis: characteristics, function, and molecular signaling, Front. Immunol. 12 (2021) 763334.
[10] Y. Wang, X. Wang, Y. Pang, X. Li, C. Gao, D. Zhang, G. Li, Y. Yu, X. Yang, Q. Cai, Ion-engineered microcryogels via osteogenesis-angiogenesis coupling and inflammation reversing augment vascularized bone regeneration, Adv. Funct. Mater. 34 (34) (2024) 2400745.
[11] S. Thamphiwatana, P. Angsantikul, T. Escajadillo, Q. Zhang, J. Olson, B.T. Luk, S. Zhang, R.H. Fang, W. Gao, V. Nizet, L. Zhang, Macrophage-like nanoparticles concurrently absorbing endotoxins and proinflammatory cytokines for sepsis management, Proc. Natl. Acad. Sci. U. S. A 114 (43) (2017) 11488–11493.
[12] H. Wang, H. Liu, J. Li, C. Liu, H. Chen, J. Li, C. Sun, T. Guo, Z. Pang, B. Zhang, Y. Hu, Cytokine nanosponges suppressing overactive macrophages and dampening systematic cytokine storm for the treatment of hemophagocytic lymphohistiocytosis, Bioact. Mater. 21 (2023) 531–546.
[13] K.Y.W. Teo, C. Sevencan, Y.A. Cheow, S. Zhang, D.T. Leong, W.S. Toh, Macrophage polarization as a facile strategy to enhance efficacy of macrophage membrane-coated nanoparticles in osteoarthritis, Small Sci. 2 (4) (2022) 2100116.
[14] Y. Cui, B. Lv, Z. Li, C. Ma, Z. Gui, Y. Geng, G. Liu, L. Sang, C. Xu, Q. Min, L. Kong, Z. Zhang, Y. Liu, X. Qi, D. Fu, Bone-targeted biomimetic nanogels Re-establish osteoblast/osteoclast balance to treat postmenopausal osteoporosis, Small 20 (6) (2024) e2303494.
[15] C. Yin, Q. Zhao, W. Li, Z. Zhao, J. Wang, T. Deng, P. Zhang, K. Shen, Z. Li, Y. Zhang, Biomimetic anti-inflammatory nano-capsule serves as a cytokine blocker and M2 polarization inducer for bone tissue repair, Acta Biomater. 102 (2020) 416–426.
[16] C. Schlundt, H. Fischer, C.H. Bucher, C. Rendenbach, G.N. Duda, K. Schmidt-Bleek, The multifaceted roles of macrophages in bone regeneration: a story of polarization, activation and time, Acta Biomater. 133 (2021) 46–57.

[17] B. Chang, N. Ahuja, C. Ma, X. Liu, Injectable scaffolds: preparation and application in dental and craniofacial regeneration. Materials Science & Engineering. R, Reports, Rev. J. 111 (2017) 1–26.
[18] Z. Yuan, P. Wei, Y. Huang, W. Zhang, F. Chen, X. Zhang, J. Mao, D. Chen, Q. Cai, X. Yang, Injectable PLGA microspheres with tunable magnesium ion release for promoting bone regeneration, Acta Biomater. 85 (2019) 294–309.
[19] Z. Yuan, Z. Wan, Z. Tian, Y. Han, X. Huang, Y. Feng, W. Xie, X. Duan, S. Huang, X. Liu, J. Huang, In situ fused granular hydrogels with ultrastretchability, strong adhesion, and mutli-bioactivities for efficient chronic wound care, Chem. Eng. J. 450 (2022) 138076.
[20] Y. Gao, Z. Yuan, X. Yuan, Z. Wan, Y. Yu, Q. Zhan, Y. Zhao, J. Han, J. Huang, C. Xiong, Q. Cai, Bioinspired porous microspheres for sustained hypoxic exosomes release and vascularized bone regeneration, Bioact. Mater. 14 (2022) 377–388.
[21] S. Jiang, H. Jing, Y. Zhuang, J. Cui, Z. Fu, D. Li, C. Zhao, U. Liaqat, K. Lin, BMSCs-laden mechanically reinforced bioactive sodium alginate composite hydrogel microspheres for minimally invasive bone repair, Carbohydr. Polym. 332 (2024) 121933.
[22] X. Yuan, Z. Yuan, Y. Wang, Z. Wan, X. Wang, S. Yu, J. Han, J. Huang, C. Xiong, L. Ge, Q. Cai, Y. Zhao, Vascularized pulp regeneration via injecting simvastatin functionalized GelMA cryogel microspheres loaded with stem cells from human exfoliated deciduous teeth, Mater. Today. Bio. 13 (2022) 100209.
[23] Z. Yuan, X. Yuan, Y. Zhao, Q. Cai, Y. Wang, R. Luo, S. Yu, Y. Wang, J. Han, L. Ge, J. Huang, C. Xiong, Injectable GelMA cryogel microspheres for modularized cell delivery and potential vascularized bone regeneration, Small 17 (11) (2021) e2006596.
[24] Z. Wan, Z. Yuan, Y. Li, Y. Zhang, Y. Wang, Y. Yu, J. Mao, Q. Cai, X. Yang, Hierarchical therapeutic ion-based microspheres with precise ratio-controlled delivery as microscaffolds for in situ vascularized bone regeneration, Adv. Funct. Mater. 32 (23) (2022) 202113280.
[25] M. Bohner, B.L.G. Santoni, N. Döbelin, β-tricalcium phosphate for bone substitution: synthesis and properties, Acta Biomater. 113 (2020) 23–41.
[26] A.H. Mahmoud, Y. Han, R. Dal-Fabbro, A. Daghrery, J. Xu, D. Kaigler, S.B. Bhaduri, J. Malda, M.C. Bottino, Nanoscale β-TCP-laden GelMA/PCL composite membrane for guided bone regeneration, ACS Appl. Mater. Interfaces 15 (27) (2023) 32121–32135.
[27] L. Zhang, Z. Wan, Z. Yuan, J. Yang, Y. Zhang, Q. Cai, J. Huang, Y. Zhao, Construction of multifunctional cell aggregates in angiogenesis and osteogenesis through incorporating hVE-cad-Fc-modified PLGA/β-TCP microparticles for enhancing bone regeneration, J. Mater. Chem. B 10 (17) (2022) 3344–3356.
[28] M. Zheng, M. Weng, X. Zhang, R. Li, Q. Tong, Z. Chen, Beta-tricalcium phosphate promotes osteogenic differentiation of bone marrow-derived mesenchymal stem cells through macrophages, Biomed. Mater. 16 (2) (2021) 025005.
[29] N. Su, C. Villicana, D. Barati, P. Freeman, Y. Luo, F. Yang, Stem cell membrane-coated microribbon scaffolds induce regenerative innate and adaptive immune responses in a critical-size cranial bone defect model, Adv. Mater. 35 (10) (2023) e2208781.
[30] C. Ding, C. Yang, T. Cheng, X. Wang, Q. Wang, R. He, S. Sang, K. Zhu, D. Xu, J. Wang, X. Liu, X. Zhang, Macrophage-biomimetic porous Se@SiO(2) nanocomposites for dual modal immunotherapy against inflammatory osteolysis, J. Nanobiotechnol. 19 (1) (2021) 382.
[31] Z. Yuan, Z. Wan, P. Wei, X. Lu, J. Mao, Q. Cai, X. Zhang, X. Yang, Dual-controlled release of icariin/Mg(2+) from biodegradable microspheres and their synergistic upregulation effect on bone regeneration, Adv. Healthcare Mater. 9 (11) (2020) e2000211.
[32] Y. Yuan, X. Shi, Z. Gan, F. Wang, Modification of porous PLGA microspheres by poly-l-lysine for use as tissue engineering scaffolds, Colloids Surf. B Biointerfaces 161 (2018) 162–168.
[33] C. Ni, J. Zhou, N. Kong, T. Bian, Y. Zhang, X. Huang, Y. Xiao, W. Yang, F. Yan, Gold nanoparticles modulate the crosstalk between macrophages and periodontal ligament cells for periodontitis treatment, Biomaterials 206 (2019) 115–132.
[34] M.B. Grauballe, J.A. Østergaard, S. Schou, A. Flyvbjerg, P. Holmstrup, Effects of TNF-α blocking on experimental periodontitis and type 2 diabetes in obese diabetic Zucker rats, J. Clin. Periodontol. 42 (9) (2015) 807–816.
[35] X.T. He, X. Li, Y. Xia, Y. Yin, R.X. Wu, H.H. Sun, F.M. Chen, Building capacity for macrophage modulation and stem cell recruitment in high-stiffness hydrogels for complex periodontal regeneration: experimental studies in vitro and in rats, Acta Biomater. 88 (2019) 162–180.
[36] M. Yu, D. Luo, J. Qiao, J. Guo, D. He, S. Jin, L. Tang, Y. Wang, X. Shi, J. Mao, S. Cui, Y. Fu, Z. Li, D. Liu, T. Zhang, C. Zhang, Z. Li, Y. Zhou, Y. Liu, A hierarchical bilayer architecture for complex tissue regeneration, Bioact. Mater. 10 (2022) 93–106.
[37] P. Jin, M. Xia, M. Hasany, P. Feng, J. Bai, J. Gao, W. Zhang, M. Mehrali, R. Wang, A tough injectable self-setting cement-based hydrogel for noninvasive bone augmentation, Interdiscipl. Mater. 2 (5) (2023) 771–788.
[38] S. McArthur, G. Juban, T. Gobbetti, T. Desgeorges, M. Theret, J. Gondin, J. E. Toller-Kawahisa, C.P. Reutelingsperger, B. Chazaud, M. Perretti, R. Mounier, Annexin A1 drives macrophage skewing to accelerate muscle regeneration through AMPK activation, J. Clin. Investig. 130 (3) (2020) 1156–1167.
[39] H. Xu, S. Zhang, A.A. Sathe, Z. Jin, J. Guan, W. Sun, C. Xing, H. Zhang, B. Yan, CCR2(+) macrophages promote orthodontic tooth movement and alveolar bone remodeling, Front. Immunol. 13 (2022) 835986.
[40] R.P. Darveau, Periodontitis: a polymicrobial disruption of host homeostasis, Nat. Rev. Microbiol. 8 (7) (2010) 481–490.
[41] Z. Chen, C. Wu, W. Gu, T. Klein, R. Crawford, Y. Xiao, Osteogenic differentiation of bone marrow MSCs by β-tricalcium phosphate stimulating macrophages via BMP2 signalling pathway, Biomaterials 35 (5) (2014) 1507–1518.
[42] S. Murphy, D. Boyd, S. Moane, M. Bennett, The effect of composition on ion release from Ca-Sr-Na-Zn-Si glass bone grafts, J. Mater. Sci. Mater. Med. 20 (11) (2009) 2207–2214.
[43] D. Zheng, W. Chen, T. Chen, X. Chen, J. Liang, H. Chen, H. Shen, L. Deng, H. Ruan, W. Cui, Hydrogen ion capturing hydrogel microspheres for reversing inflammaging, Adv. Mater. 36 (5) (2024) e2306105.
[44] F. Liu, H. Qiu, M. Xue, S. Zhang, X. Zhang, J. Xu, J. Chen, Y. Yang, J. Xie, MSC-secreted TGF-β regulates lipopolysaccharide-stimulated macrophage M2-like polarization via the Akt/FoxO1 pathway, Stem Cell Res. Ther. 10 (1) (2019) 345.
[45] M. Zhao, Q. Yang, S. Zhang, C. Zhang, Z. Wu, Enhancing bone regeneration with a novel bioactive glass-functionalized polyetheretherketone scaffold by regulating the immune microenvironment, Smart Mater. Med. 5 (1) (2024) 92–105.
[46] X. Li, Y. Jiang, X. Liu, J. Fu, J. Du, Z. Luo, J. Xu, U.K. Bhawal, Y. Liu, L. Guo, Mesenchymal stem cell-derived apoptotic bodies alleviate alveolar bone destruction by regulating osteoclast differentiation and function, Int. J. Oral Sci. 15 (1) (2023) 51.
[47] J.M. Kim, C. Lin, Z. Stavre, M.B. Greenblatt, J.H. Shim, Osteoblast-osteoclast communication and bone homeostasis, Cells 9 (9) (2020) 2073.
[48] C. Martins, F. Sousa, F. Araújo, B. Sarmento, Functionalizing PLGA and PLGA derivatives for drug delivery and tissue regeneration applications, Adv. Healthcare Mater. 7 (1) (2018) 1701035.
[49] L. Gu, R. Huang, N. Ni, R. Zhou, Y. Su, P. Gu, D. Zhang, X. Fan, Mg-Cross-Linked alginate hydrogel induces BMSC/macrophage crosstalk to enhance bone tissue regeneration via dual promotion of the ligand-receptor pairing of the OSM/miR-370-3p-gp130 signaling pathway, ACS Appl. Mater. Interfaces 16 (24) (2024) 30685–30702.
[50] X. Yuan, W. Yang, Y. Fu, Z. Tao, L. Xiao, Q. Zheng, D. Wu, M. Zhang, L. Li, Z. Lu, Y. Wu, J. Gao, Y. Li, Four-arm polymer-guided formation of curcumin-loaded flower-like porous microspheres as injectable cell carriers for diabetic wound healing, Adv. Healthcare Mater. 12 (30) (2023) e2301486.
[51] Z. Jiang, S. Qin, W. Wang, T. Du, Y. Zang, Y. He, X. Dong, H. Liu, G. Ma, Investigating the anti-inflammatory and bone repair-promoting effects of an injectable porous hydrogel containing magnesium ions in a rat periodontitis mode, Smart Mater. Med. 5 (2) (2024) 207–220.